

Error Estimation Criteria to Couple the Immersed Boundary Method with an Automated Adaptive Grid Algorithm

Hugo Daniel da Silva Domingos
hugo.domingos@ist.utl.pt

Instituto Superior Técnico, Universidade de Lisboa, Lisboa, Portugal

May 2017

Abstract

In this work, the results of the Immersed Boundary Method were validated and verified for bi-dimensional cases of incompressible flow. An automated adaptive grid algorithm based on error estimators was also tested. Two different error estimators were used, the Taylor criterion and the Residual one.

A study of an immersed cylinder in a flow was also performed, allowing for a comparative study between the obtained results with others from the literature, allowing to understand how the domain size influences the numerical results due to the blockage effect. A case with an analytical solution was also studied, which was ideal for the comparison of three different pairs of numerical schemes and to choose the best one to be used throughout the rest of the work.

After completing the verification of the method and the influence of numerical schemes on the results' accuracy, the IBM coupled with the automated adaptive grid algorithm had to be tested in cases with no analytical solution. To achieve this, the immersed cylinder case was studied once again, demonstrating the computational power savings that the adaptive grid brought when compared to the uniform refinement case. The accuracy of the results was also compared with the previous results. Finally, this method was also tested in a NACA 0012 airfoil.

By comparing the different results it was possible to conclude that the error estimators implementation would effectively reduce the computational power needed to achieve accurate results.

Keywords: Immersed Boundary Method (IBM), Adaptive grid generator, Error estimators, Taylor criterion, Residual criterion

1. Introduction

Over the last decades, the Cartesian grid method has been gaining popularity. In this method, the governing equations are discretized in a Cartesian grid which does not adapt to the immersed boundaries. This allows for simpler and faster grid generation and maintains the simplicity of the governing equations in Cartesian coordinates [1].

One example of a method that uses a Cartesian grid generator is the Immersed Boundary Method (IBM). The IBM was first introduced by Peskin [2] in order to study the blood flow in heart valves. This is a moving boundary problem where the blood flow simulation was performed on a Cartesian grid that did not follow the boundary geometry [3].

From the information gathered, it becomes evident that despite the high accuracy of body-fitted methods there has been a great effort to develop the IBM. Mainly, that comes from a need to reduce computational times since they play a huge role in the decision of how to discretize a domain. Having established the superiority of IBM in the grid

generation process, there is a need to develop and improve this method's accuracy and also automate the solution process.

2. Numerical Methods

The numerical method present in this work was developed in the LASEF research laboratory of Instituto Superior Técnico. This work serves as a combination of [4] where the Immersed Boundary Method was implemented and of [5] where the error estimation criteria was implemented to body-fit grids.

2.1. Governing Equations

The Navier-Stokes equations are the four partial differential equations that are used to represent the behaviour of fluids. For this the purpose of this work, compressibility properties won't be taken into account and the flow is considered to be isothermal and bi-dimensional. These simplifications result in Equations 1 and 2 which are the Navier-Stokes equations for incompressible flows.

$$\nabla \cdot \mathbf{u} = 0 \quad (1)$$

$$\frac{\partial \mathbf{u}}{\partial t} + \nabla \cdot (\mathbf{u} \otimes \mathbf{u}) = \nabla \cdot (\nu \nabla \mathbf{u}) - \frac{1}{\rho} \nabla p \quad (2)$$

2.2. Discretization Schemes

Different numerical schemes were used for uniform and adaptive refinements. The different levels of refinement present in the adaptive grid made the use of more complex schemes necessary.

The linear interpolation was used only in the study-cases where the uniform criterion refinement was used. This interpolation is done by computing the intersection point \mathbf{z}_f between the surface plane of the cell face f with Equation 3.

$$\mathbf{z}_f = \mathbf{P}_0 + \eta_{LIN}(\mathbf{P}_1 - \mathbf{P}_0) = \mathbf{P}_0 + \eta_{LIN}\mathbf{d} \quad (3)$$

Vector \mathbf{d} is the distance between cells P_0 and P_1 centroids and the blending factor η_{LIN} is calculated using the projection of $(\mathbf{f} - \mathbf{P}_0)$ and \mathbf{d} vectors to the face normal which results in Equation 4.

$$\eta_{LIN} = \frac{(\mathbf{f} - \mathbf{P}_0) \cdot \mathbf{S}_f}{\mathbf{S}_f \cdot \mathbf{S}_f} = \frac{(\mathbf{f} - \mathbf{P}_0) \cdot \mathbf{S}_f}{(\mathbf{P}_1 - \mathbf{P}_0) \cdot \mathbf{S}_f} \quad (4)$$

The diffusive scheme, used only in uniform refinement cases, consists in computing the value of the dependent variable gradient $\nabla\phi$ at the face centroid \mathbf{f} using the information from surrounding cells. The central difference scheme used has a second-order accuracy and the gradient $(\nabla\phi)_f$ is calculated with Equation 5 using two points.

$$(\nabla\phi)_f = (\phi_{P_1} - \phi_{P_0}) \frac{\mathbf{d}}{\mathbf{d} \cdot \mathbf{d}} \quad (5)$$

The schemes used for the unstructured grids that resulted from the adaptive refinement were created using the WLS method. These schemes were built using linear polynomial centred in the face centroid with the computational values of the neighbour cells.

$$\phi(\mathbf{x}) = \phi_f + (\nabla\phi)_f \cdot (\mathbf{x} - \mathbf{f}) \quad (6)$$

where ϕ_f and $(\nabla\phi)_f$ are the convective and diffusive values, respectively, so both can be computed in the same regression. The cells included in this type of regression have at least one of the face vertices.

To improve the accuracy of the schemes at non-structured grids or to compute the gradient terms of the governing equations, the variables gradients $\nabla\phi$ at the cell's centre have to be computed. The Gauss method was used in order to calculate these

gradients. The computation of ϕ_f is made using the convective scheme of Equation 3 or of Equation 6.

The continuity and momentum equations are coupled and there needs to exist an algorithm to handle the coupling of pressure and velocity. The choice of this algorithm is important because it can affect the accuracy and stability of the solution.

SIMPLE and PISO are the two different algorithms that are usually used in this situation. Despite PISO offering faster convergence speeds [6], the algorithm used in this work is the SIMPLE. The main advantage of this algorithm is being more robust which is important since the local refinement will cause a non-smooth grid locally which would cause the problem to diverge when using the PISO algorithm. This algorithm has been extensively detailed in several works like [7] and [6].

2.3. Immersed Boundary Method

The first step to implement the IB method is to divide each type of cell into three different groups according to the location of their vertices. Cells with all their vertices located in the fluid zone are called fluid cells, similarly, cells with all their vertices located in the solid zone are called solid cells, and finally, cells that have vertices located in both fluid and solid zones are called ib cells. An ib cell's face that is shared with a fluid cell is called an ib face.

The fluid cells are isolated from the remaining cells, creating an immersed boundary containing all ib faces. To this boundary is then applied a Dirichlet boundary condition for velocity and a Neumann boundary condition for the pressure correction.

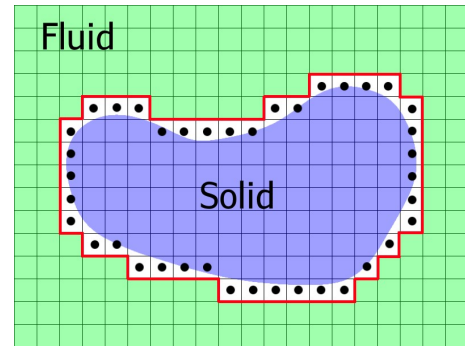


Figure 1: Conservative cut around a solid body in a Cartesian grid. [6]

2.4. Error Estimation criteria

The two different error estimation criteria that will be used in the course of this work are the Taylor and Residual ones. The purpose of these criteria is to estimate the error and the areas to be refined.

The Taylor criterion is calculated with Equation:

$$E_T = \frac{1}{2V_P} \left| \left(\frac{\partial^2 \phi}{\partial x_i \partial x_j} \right)_P \right| (M_{ij})_P \quad (7)$$

where E_T is the Taylor series based error estimation, V_P is the cell P volume, $(M_{ij})_P$ is the cell P inertia tensor and $\left| \left(\frac{\partial^2 \phi}{\partial x_i \partial x_j} \right)_P \right|$ is the Hessian matrix.

The accuracy of the error estimation is dependent on the values of the Hessian matrix according to Equation 7. The components of this matrix were based on placing the values of the closest solid point in the face of the immersed boundary. This is a very simplistic approximation. To improve the accuracy of the criterion, the accuracy of the Hessian matrix must be improved. To do that, the values were changed to the values calculated by a second order interpolation introduced by [8]. The new values to be included in the Hessian matrix can be calculated with:

$$\frac{\partial^2 u}{\partial x^2} = 2a_3 + 2a_6 y \quad (8)$$

$$\frac{\partial^2 u}{\partial y^2} = 2a_4 \quad (9)$$

$$\frac{\partial^2 v}{\partial x^2} = 2b_3 \quad (10)$$

$$\frac{\partial^2 v}{\partial y^2} = -a_5 - 2a_6 x \quad (11)$$

where a_i and b_i are the least-squares coefficients.

In order to calculate the Residual criterion, a cubic order polynomial regression is computed with the information from the first and second neighbours by vertex. With this regression, new values are computed for the cell's face and gradients. These new values will then be compared to the values obtained with the diffusive and convective schemes. Computing again the residual values using Equation 12 allows for this comparison.

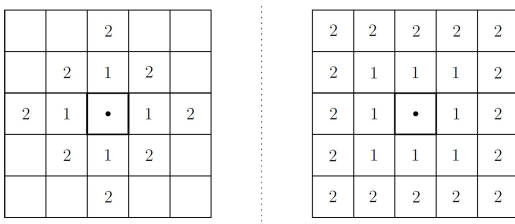


Figure 2: Example of a cell's first and second neighbours by vertex on the left and by face on the right [9].

$$E_R = \frac{\sum_{f=1}^F U_f^n u_f - \nu_f \sum_{f=1}^F (\nabla u)_f \cdot S_f}{a_p} + \frac{(V_p/\rho) \nabla p^n}{a_p} \quad (12)$$

where u_f and $(\nabla u)_f$ values are computed with the cubic regression and a_p is the value of the matrix used for the momentum equations.

2.5. Adaptive Meshing Algorithm

Since a refinement step divides the hydraulic diameter in half, it is possible to achieve a relation between the error on two different refinement levels in:

$$E_0/E \sim (h_i/h)^2 = (1/2)^2 = 0.25 \quad (13)$$

The maximum value for the error estimation is then chosen and multiplied by the error reduction factor of 0.25 calculated in 13. The result of this product is the threshold for whether or not the cells are refined. All cells with an error estimation higher than the threshold are selected and will be refined.

When applied to coarse grids, this type of refinement can result in a stiff cell distribution which can then cause numerical instabilities and divergence. This problem becomes more evident with the increasing number of refinement levels. To improve the general quality of the mesh and to try and avoid these problems, some measures are taken:

- The results for the criterion are smoothed in the domain;
- The selection of cells to be refined is expanded to their neighbour cells;
- If in a group of cells chosen to be refined, there are cells with different refinement levels, only the ones with the lowest level will be refined, preventing the accumulation of grid interface in the same location;
- The refinement directions are cross-checked. This causes incompatible directions of refinement to be excluded;
- As the anisotropic cells stretch, it is harder to refine them in counter direction. This prevents the degree of non-orthogonality to become severe.

This algorithm plays a vital role for this project because achieving an accurate solution is dependent on a grid that does not cause numerical instabilities or that causes the solution to diverge.

3. Verification and Validation

The code used to perform the simulations of a flow past an immersed body is compared with other solutions from other works, and its validity is tested using an array of cases.

3.1. Flow Around a 2D Cylinder

Flow past a circular cylinder is one of the most studied problems in fluid mechanics due to its geometric characteristics and practical importance in

engineering [10]. These reasons made this a benchmark problem with a vast amount of data from both experimental and numerical data in the literature. Flow characteristics and drag coefficient on the cylinder are dependent on the Reynolds number. The Reynolds number is the ratio between inertial and viscous forces and can be calculated for this case study with:

$$Re = \frac{U_\infty D}{\nu} \quad (14)$$

where U_∞ is the velocity at the inlet boundary, D the diameter of the cylinder and ν is the kinematic viscosity of the fluid. The drag coefficient can be calculated with:

$$C_D = \frac{2F_D}{\rho U_\infty^2 A_{proj}} \quad (15)$$

where F_D is the drag force, ρ is the fluid density and A_{proj} is the projected area of the cylinder perpendicular to the flow ($A_{proj} = D$). Three different Reynolds numbers were chosen to compare with the literature available ($Re = 10$, $Re = 20$ and $Re = 40$).

After analysing the range of results in the literature for the case of an immersed cylinder, it was obvious they were inconsistent. One of the reasons why results differed so much from one another may be because of different domain sizes that caused different values of the blockage effect, impacting the final results.

The blockage effect is created by immersing a cylinder in a flow can alter significantly the results obtained due to the flow confinement. The blockage factor is the ratio between the diameter (D) and half the height (h) of the domain ($B = D/h$) and its effect is considered to be insignificant when $B \leq 0.01$ [11].

To confirm the effects of the blockage effect, a study using the in-house code was done. It was decided to use a body-fit grid because this code was already tested and this effect should not vary between different methods. After several simulations for four different domain sizes and respective blockage values, the results can be presented in Figure 3 and Table 1. The percentage error in Table 1 is calculated comparing the results from each grid size to the grid with the biggest domain.

To perform this study, a very refined grid was used for $B=0.01$. Cutting the grid or adding new cells was required in order to generate grids with the same characteristics but different values for B .

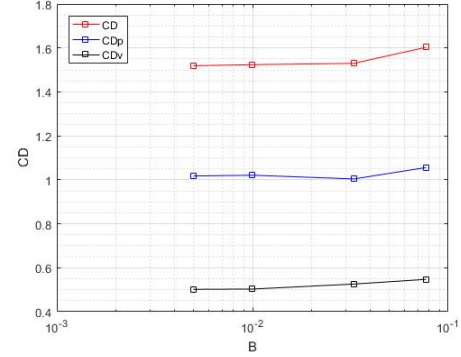


Figure 3: Variation of the drag coefficient with the blockage effect for $Re = 40$ in a body-fit grid with the in-house code.

Table 1: Drag coefficient with the respective viscous and pressure components variation with the blockage effect

	Blockage			
	0.077	0.033	0.01	0.005
C_D	1.6028	1.5297	1.5237	1.5191
C_{Dp}	1.0558	1.0041	1.0208	1.0174
C_{Dv}	0.546971	0.525806	0.5029	0.5017
Error (%)	5.512488	0.7098	0.3058	-

It is now obvious from the previous results that the conclusion from [11] is also valid for this work and because of that, the domain size to be studied from this point forward, shall respect the condition $B = 0.01$ since lower values do not significantly improve the results.

Having performed several numerical analyses, it is now possible to focus on one specific Reynolds number at a time. In this section, a comparison between the achieved results and literature results will be made.

Figure 4 presents the flow past the immersed body. In this Figure it can be easily surmised that the size of the eddies behind the solid body are very small.

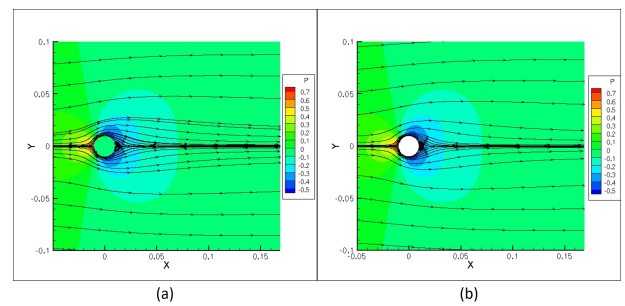


Figure 4: Pressure distribution with velocity streamlines in the IBM(a) and in the Body-fit Method (b) for $Re = 10$.

Table 2 summarizes the results from different authors. L_w/D is the quotient between the wake's length and the diameter of the immersed body. None of these works studied the effect of the blockage effect, and because of that, it is important to understand what were the domain characteristics for each work in order to have a better sense of why some values differ from one to another. A more detailed table is available in the appendix where more details can be found.

Table 2: Results from literature survey and from the present work for $Re = 10$.

Reference	year	L_w/D	C_D	B
Lima E Silva et al. [12]	2003	0.26	2.81	-
He and Doolen [13]	1997	0.24	3.17	0.018
Sen et al. [11]	2009	-	2.795	-
Ding et al. [14]	2004	0.252	3.07	0.03125
Park et al. [10]	1998	-	2.78	0.02
Present - Bodyfit	2016	-	2.78	0.01
Present work - STAR-CCM+	2016	-	2.82	0.025
Present work - IBM	2016	-	2.75	0.01

As expected, values from the present work fall in the range of results calculated by other authors.

Having performed a comparative analysis for $Re = 10$, it is now time to do the same for $Re = 20$. Similarly to the previous section, the first step is to do a visual analysis of the results from both IB and Body-fit methods.

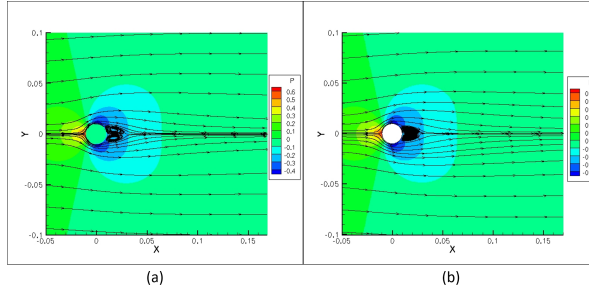


Figure 5: Pressure distribution with velocity streamlines in the IBM(a) and in the Body-fit Method (b) for $Re = 20$.

As expected, in Figure 5 it is obvious the growth in the eddies' size. This behaviour falls in line with what was previously stated about the relation between Reynolds number and the size of the eddies.

Table 3 summarizes all the results obtained from the literature survey as well as with the information about the blockage effect and L_w/D .

Table 3: Results from literature survey and from the present work for $Re = 20$

Reference	year	L_w/D	C_D	B
Lima E Silva et al. [12]	2003	1.04	2.04	-
Ye et al. [1]	1999	0.92	2.03	-
Linnick and Fasel [15]	2005	0.93	2.16	0.056
Linnick and Fasel [15]	2005	0.93	2.06	0.023
Fornberg [16]	1980	0.91	2	-
Calhoun [17]	2002	0.91	2.19	-
Niu et al. [18]	2006	0.95	2.144	0.025
He and Doolen [13]	1997	0.92	2.152	0.018
Wang et al. [3]	2009	0.98	2.25	0.067
Xu and Wang [19]	2006	0.92	2.23	0.0625
Choi et al [20]	2007	0.9	2.02	0.0125
Pacheco et al. [21]	2005	0.91	2.08	0.033
Frisani and Hassan [22]	2015	0.9	2.22	0.05
Frisani and Hassan [22]	2015	0.93	2.229	0.05
Frisani and Hassan [22]	2015	0.85	2.168	0.05
Frisani and Hassan [22]	2015	0.92	2.124	0.05
Frisani and Hassan [22]	2015	0.92	2.167	0.05
Sen et al. [11]	2009	-	2.019	-
Ding et al.[14]	2004	0.93	2.18	0.03125
Park et al. [10]	1998	-	2.01	0.02
Present work- Bodyfit	2016	-	2.01	0.01
Present work - STAR-CCM+	2016	-	2.04	0.025
Present WORK - IBM	2016	-	1.99	0.01

Once again, the results obtained in the course of this work are similar to the values obtained by other works when a similar B is being used.

Finally, $Re = 40$ also requires the type of analysis already performed for the other Reynolds numbers.

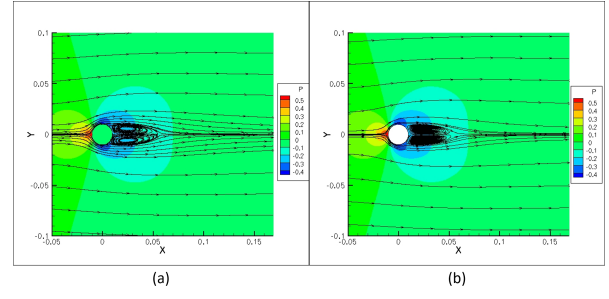


Figure 6: Pressure distribution with velocity streamlines in the IBM(a) and in the Body-fit Method (b) for $Re = 40$.

In Figure 6 the size of the eddies becomes even larger comparing it with the $Re = 10$ and $Re = 20$. Once again, Table 4 summarizes all the results from the literature.

In this last case, the results for the drag coefficient can also be verified since they fall under the values from other authors.

There are several conclusions that can be made from this case. The domain size to study is very important, and by observing the results from the comparative table with the literature results for each Reynolds it becomes evident that the disparity of values can be caused by the different blockage values. It is simply not enough to perform analysis with a domain size chosen by comparison with other work. The error this effect can have in the results

Table 4: Results from literature survey and from the present work for $Re = 40$

Reference	year	L_w/D	C_D	B
Lima E Silva et al. [12]	2003	2.55	1.54	-
Ye et al. [1]	1999	2.27	1.52	-
Linnick and Fasel [15]	2005	2.23	1.61	0.056
Linnick and Fasel [15]	2005	2.23	1.54	0.023
Fornberg [16]	1980	2.24	1.5	-
Calhoun [17]	2002	2.18	1.62	-
Niu et al. [18]	2006	2.26	1.589	0.025
He and Doolen [13]	1997	2.25	1.499	0.018
Wang et al. [3]	2009	2.35	1.66	0.067
Xu and Wang [19]	2006	2.21	1.66	0.0625
Choi et al [20]	2007	2.25	1.52	0.0125
Pacheco et al. [21]	2005	2.28	1.53	0.033
Tseng and Ferziger [23]	2003	2.21	1.53	0.0625
Mittal et al. [24]	2008	-	1.53	0.025
Kim et al. [25]	2001	-	1.51	0.01
Frisani and Hassan [22]	2015	2.4	1.661	0.05
Frisani and Hassan [22]	2015	2.35	1.656	0.05
Frisani and Hassan [22]	2015	2.09	1.615	0.05
Frisani and Hassan [22]	2015	2.29	1.587	0.05
Frisani and Hassan [22]	2015	2.4	1.611	0.05
Sen et al. [11]	2009	-	1.514	-
Ding et al.[14]	2004	2.2	1.713	0.03125
Park et al. [10]	1998	-	1.51	0.02
Present work - Bodyfit	2016	-	1.50	$B = 0.01$
Present work - STAR-CCM+	2016	-	1.53	0.025
Present work - IBM	2016	-	1.49	0.01

is large, so it is always necessary to try and make a compromise between domain size and computational power available for simulations.

It is also important to note that the IBM has more difficulties converging when a uniform refinement is performed when compared with a body-fit method. The computational power and time required in this case did not justify continuing the uniform refinement of the grid.

3.2. Analytical Singularity

The analytical case chosen to study was the placement of a singularity inside a cylinder with a radius of 0.1 in the middle of a squared domain (1×1). This problem has an exact solution of the Navier-Stokes equations, which makes it ideal to test the IBM. The Reynolds number chosen to perform this analysis is $Re = 1000$. The decision of the problem to study and the Reynolds number was made following the work done in [26] and [27]. The equations that characterized the problem were altered in order to place the singularity inside the domain. The new equations 16, 17 and 18 give the exact solution for the horizontal, vertical velocities and pressure, respectively.

$$u = -\frac{2 \times (y - 0.5)}{(x - 0.5)^2 + (y - 0.5)^2}, \quad (16)$$

$$v = \frac{2 \times (x - 0.5)}{(x - 0.5)^2 + (y - 0.5)^2}, \quad (17)$$

$$p = -\frac{2}{(x - 0.5)^2 + (y - 0.5)^2}, \quad (18)$$

where x and y are the Cartesian coordinates.

The adaptive grids obtained at the final levels of refinement for each criterion are shown in Figure 7.

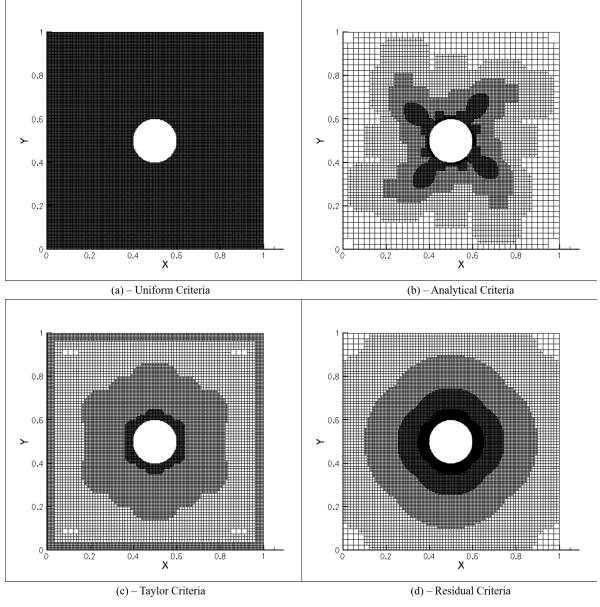


Figure 7: Analytical Singularity: Final grids for the different criteria.

The error distribution in Figure 8 has a higher concentration in the diagonal region near the cylinder. One important thing to note from error estimation distribution from Figure 8 is that the Taylor criterion over-estimated the error in the computational boundary. This will lead to an increase in the cells number, decreasing the computational efficiency.

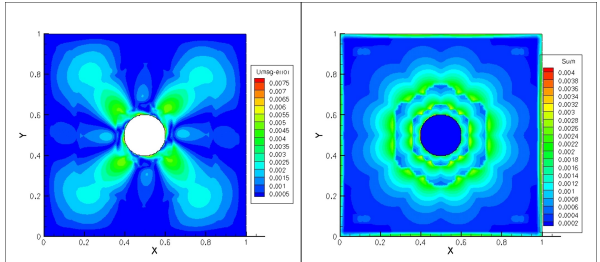


Figure 8: Analytical Singularity - Velocity magnitude error field on the left and error estimation criterion values on the right for the level 8 of the Taylor criterion.

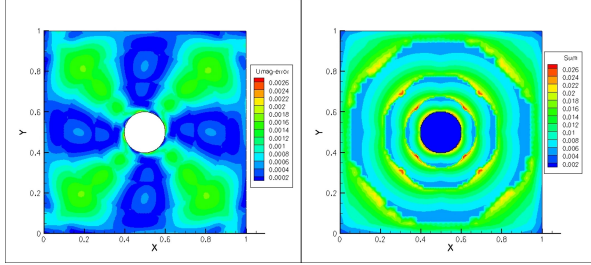


Figure 9: Analytical Singularity - Velocity magnitude error field on the left and error estimation criterion values on the right for the level 7 of the Residual criterion.

From the error estimation distribution for the Residual criterion, it is possible to see that this criterion is better at detecting the error in the diagonals of the domain and that it does not overestimate the error in the computational boundaries.

For a better comparison between each criterion, a measure of efficiency should be used. The measure chosen is the ratio between mean and maximum errors. In Table 5 the efficiency values for the most refined grids of each error estimation criteria can be analysed. The uniform criterion is the one with the lowest efficiency and the analytical one has the highest efficiency as expected. The real comparison is between the Taylor and Residual error estimators and the Residual criterion seems to be far more efficient.

Table 5: Analytical Singularity: Efficiency Values for the most refined grid of each criteria.

	μ_u	μ_{mag}
Uniform criterion	0.0352	0.058
Analytical Criterion	0.305	0.384
Taylor Criterion	0.084	0.14
Residual Criterion	0.197	0.252

In Figure 10 a comparison between criteria is presented. The analytical adaptive criterion is the best at lowering the maximum error but both error estimation criteria exhibit a similar behaviour, evidencing their good capabilities in reducing the computational error.

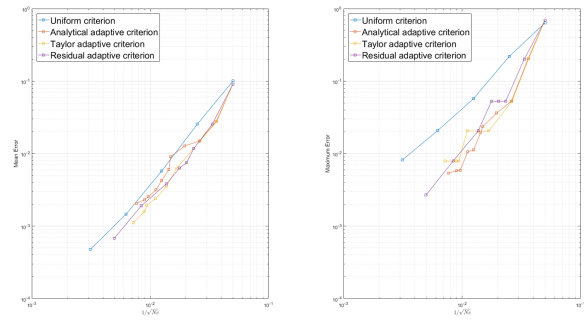


Figure 10: Analytical Singularity - Comparison between the different criteria of the error decay with $1/\sqrt{N_c}$.

This case-study is also a good opportunity to compare the diffusive and convective schemes used with others available in the SOL code. Figure 11 presents the results for the analytical adaptive criteria with different schemes. The GPS is the ghost points family scheme, the FLS uses the Face Least Squares scheme and the pair GQS uses a Least Squares scheme for the diffusion and a triangular interpolation with skewness correction as the convection scheme.

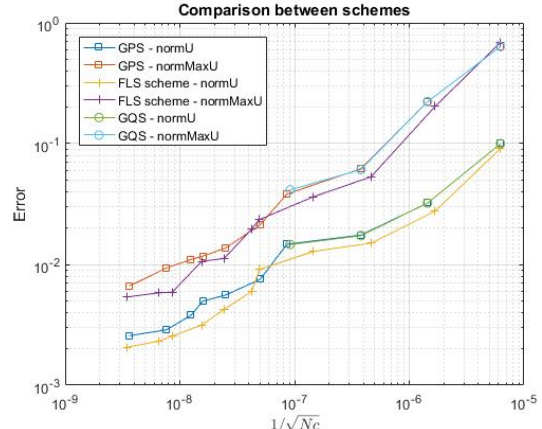


Figure 11: Analytical Singularity - Comparison between schemes for the analytical criterion.

After a simple analysis of Figure 11 the FLS scheme is clearly proven to be a better choice for performing all the computational analyses with adaptive grids since the decrease in error is more evident with this scheme and it does not have the same instability problem of pair GQS that caused the simulation to diverge.

4. Results

The main purpose of this work was to implement an automatic refinement criteria that would be able to reduce the computational power needed to achieve accurate solutions using the Immersed Boundary

method. In the previous chapter, these criteria were compared with computational methods from other works and with analytical solutions, where it's possible to conclude that these error estimation criteria allow for solutions with a better grid convergence, improving the capabilities of the initial IBM. In the present chapter, the results with the verified adaptive algorithm for different flows will be presented.

4.1. Flow around a 2D cylinder with Adaptive Criteria

This is the case already introduced in Section 3.1 but now tested with adaptive grids.

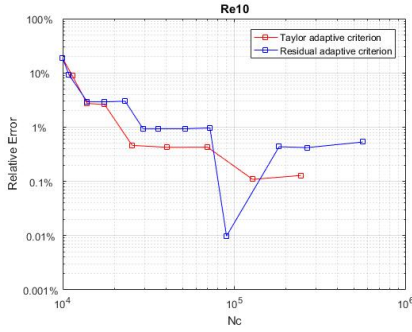


Figure 12: Relative error between both adaptive criteria and the body-fit method for $Re = 10$.

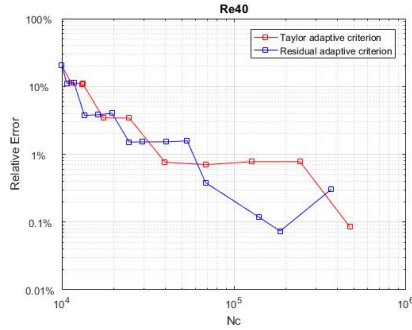


Figure 13: Relative error between both adaptive criteria and the body-fit method for $Re = 40$.

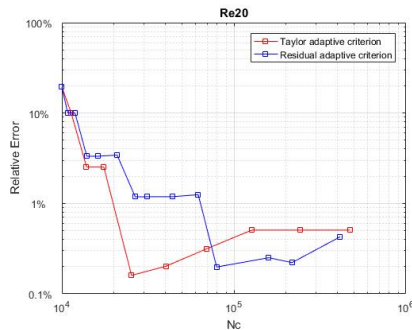


Figure 14: Relative error between both adaptive criteria and the body-fit method for $Re = 20$.

In Figure 12 it is possible to see how the drag coefficient error converges with the increase in cell's numbers. Both criteria are fast to converge but the Residual adaptive criteria does not over-estimate the error in the computational boundaries and it refines a more broader area of the cylinder. The Taylor adaptive criterion on the other hand, adds unnecessary cells to the computational boundary and the refinement in the cylinder zone is less smooth. The same conclusions as for $Re = 10$ can be made for Figure 14 but now, the Taylor adaptive criterion is even faster to converge. In Figure 13 it becomes more apparent the values obtained through the Taylor adaptive criterion tend to approximate those of the Residual adaptive criterion with the increase in number of cells. One of the reasons why the Taylor adaptive criterion needs a larger number of cells is the unnecessary refinement in the computational boundaries.

4.2. Flow Around the NACA 0012 airfoil

Figures 15 - 17 summarize the results for the IBM with the different criteria used by comparing them to the results from the most refined body-fit grid. The lift coefficient for $\alpha = 0^\circ$ was not compared since it is approximately zero as expected.

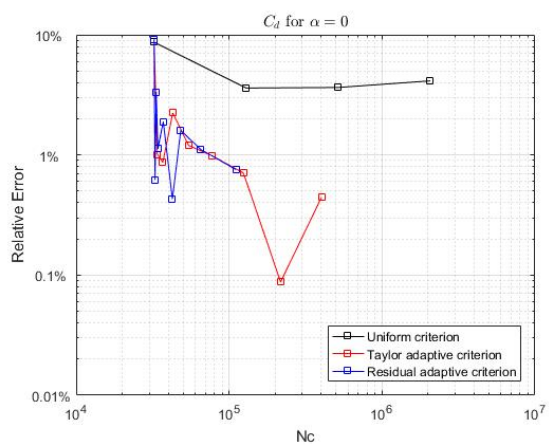


Figure 15: C_d error relative to the body-fit method for $\alpha = 0^\circ$.

The uniform criterion has a 2.37% error when compared to the most refined grid of the body-fit method. Both criteria have also failed to converge to a clear result before instabilities in the grid caused the simulation to diverge. Despite this, the results have a relative error lower than 1% when compared to the body-fit method.

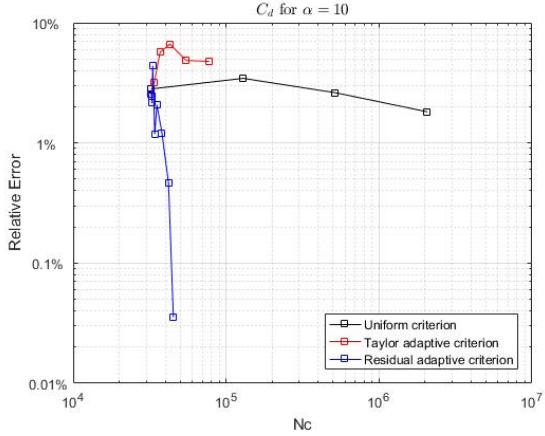


Figure 16: C_d error relative to the body-fit method for $\alpha = 10^\circ$.

The uniform criterion of the IBM has failed to converge despite the high number of cells. For this attack angle, the Residual adaptive criterion simulation resulted in a 0.04% error when compared to the body-fit method. More refinement levels should be used for a more clear convergence of this method, but the instabilities in the simulation caused it to diverge. Despite the lack of more refinement levels, the error between the two final levels for this criterion is only 0.43%. The Taylor criterion has converged for a 4.77% error.

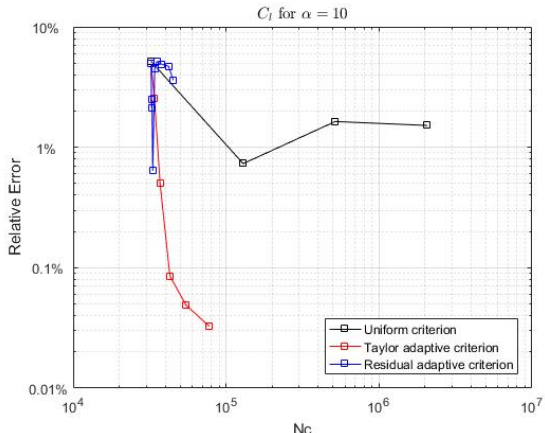


Figure 17: C_l error relative to the body-fit method for $\alpha = 10^\circ$.

The Taylor criterion has a small error value of 0.03%. The Residual criterion on the other hand has the largest error of 3.6% but it is still to converge. Once again, more levels of refinement for the Residual criterion would be useful, however the simulation failed to converge after the present results.

A possible justification for the difference in results for $\alpha = 10^\circ$ is that the flow for this angle of attack is unsteady. The literature is clear that for

$\alpha = 0^\circ$ the flow is steady, however for $\alpha = 10^\circ$ there is not a consensus and the flow may have become unsteady causing the differences in values between the error criteria and the body-fit method.

5. Conclusions

In this work, an extensive study of the IBM results was made with the purpose of verifying and validating the method by comparison with other works. After validating the method, the error estimation criteria could then be applied and the results compared to see the benefits these criteria bring. Implementing these criteria to generate adaptive grids allowed a great reduction in the computational power needed to successfully simulate flows.

An extensive study of an immersed 2D cylinder case was made for $Re = 10$, $Re = 20$ and $Re = 40$ both with and without the adaptive criteria. This served as an ideal example to show the capabilities of an automated adaptive grid algorithm coupled with the error estimation criteria since it demonstrated how much computational power could be saved.

Finally, the IBM with adaptive refinement was also applied to a NACA 0012 airfoil. This case proved more of a challenge for both body-fit and IBM generated grids.

With the studies performed in this Thesis, it is clear the benefits in terms of accuracy and computational power both criteria brought to the IBM. The Residual error estimator proved to be a better criteria, with more efficient adaptive grids and smooth refined areas. The Taylor error estimator on the other hand had some instability problems caused by non-smooth grids and it also over-estimated error in the computational boundary, adding unnecessary cells to the grids, and therefore increasing the computational power need to solve each simulation.

References

- [1] T Ye, R Mittal, H S Udaykumar, and W Shyy. An Accurate Cartesian Grid Method for Viscous Incompressible Flows with Complex Immersed Boundaries. *Journal of Computational Physics*, 156:209–240, 1999.
- [2] Cs Peskin. Numerical analysis of blood flow in the heart. *Journal of Computational Physics*, 25:220–252, 1977.
- [3] Zeli Wang, Jianren Fan, and Kefa Cen. Immersed boundary method for the simulation of 2D viscous flow based on vorticity velocity formulations. *Journal of Computational Physics*, 228(5):1504–1520, 2009.
- [4] Jonas Alexandre, Silva Pereira, Supervisors José, and Carlos Fernandes. *A 2-D Immersed Boundary Method on Low Reynolds Moving Body*. PhD thesis, 2014.
- [5] Duarte M. S. Albuquerque, José M. C. Pereira, and José C. F. Pereira. Residual Least-Squares Error Estimate for Unstructured h-Adaptive Meshes. *Numerical Heat Transfer, Part B: Fundamentals*, 67(3):187–210, 2014.
- [6] Diogo Matias and Coimbra Martins. On the suppression of spurious pressure oscillations in immersed boundary methods with unstructured grids. (November), 2016.

- [7] Albuquerque, Duarte. *Numerical Computation of Incompressible Flows on Adaptive and Unstructured Grids*. PhD thesis, 2013.
- [8] Lin Sun, Sanjay R. Mathur, and Jayathi Y. Murthy. An Unstructured Finite-Volume Method for Incompressible Flows with Complex Immersed Boundaries. *Numerical Heat Transfer, Part B: Fundamentals*, 58(4):217–241, 2010.
- [9] Joo Magalhes, Silva Pereira, Supervisors José, and Carlos Fernandes. *An adaptive framework for the numerical simulation of environmental flows in complex geometries*. PhD thesis, 2011.
- [10] Jeongyoung Park, Kiyoung Kwon, and Haecheon Choi. Numerical solutions of flow past a circular cylinder at Reynolds numbers up to 160. *KSME International Journal*, 12(6):1200–1205, 1998.
- [11] Subhankar Sen, Sanjay Mittal, and Gautam Biswas. Steady separated flow past a circular cylinder at low Reynolds numbers. *Journal of Fluid Mechanics*, 620:89, 2009.
- [12] A L F Lima E Silva. Numerical simulation of two-dimensional flows over a circular cylinder using the immersed boundary method. *Journal of Computational Physics*, 189:351–370, 2003.
- [13] Xiaoyi He and Gary Doolen. Lattice Boltzmann Method on Curvilinear Coordinates System: Flow around a Circular Cylinder. *Journal of Computational Physics*, 134:306–315, 1997.
- [14] H. Ding, C. Shu, K.S. Yeo, and D. Xu. Simulation of incompressible viscous flows past a circular cylinder by hybrid FD scheme and meshless least square-based finite difference method. *Computer Methods in Applied Mechanics and Engineering*, 193(9-11):727–744, 2004.
- [15] Mark N Linnick and Hermann F Fasel. A high-order immersed interface method for simulating unsteady incompressible flows on irregular domains. *Journal of Computational Physics*, 204:157–192, 2005.
- [16] Bengt Fornberg. A numerical study of steady viscous flow past a circular cylinder. *Journal of Fluid Mechanics*, 98:819–855, 1980.
- [17] Donna Calhoun. A Cartesian Grid Method for Solving the Equations in Irregular Regions. *Journal of Computational Physics*, 176:231–275, 2002.
- [18] X D Niu, C Shu, Y T Chew, and Y Peng. A momentum exchange-based immersed boundary-lattice Boltzmann method for simulating incompressible viscous flows. *Physics Letters A*, 354:173–182, 2006.
- [19] Sheng Xu and Z Jane Wang. An immersed interface method for simulating the interaction of a fluid with moving boundaries. *Journal of Computational Physics*, 2006.
- [20] Jung-il Choi, Roshan C Oberoi, Jack R Edwards, and Jacky A Rosati. An immersed boundary method for complex incompressible flows. *Journal of Computational Physics*, 224:757–784, 2007.
- [21] R E Peck, J R Pacheco, T Rodic, and San Luis Potos. Numerical simulations of heat transfer and fluid flow problems using an Immersed-Boundary Finite-Volume method on nonstaggered grids. *Numerical Heat Transfer, Part B: Fundamentals*, 47:1–24, 2005.
- [22] Angelo Frisani and Yassin A. Hassan. On the immersed boundary method: Finite element versus finite volume approach. *Computers & Fluids*, 121:51–67, 2015.
- [23] Yuheng Tseng and Joel H Ferziger. A ghost-cell immersed boundary method for flow in complex geometry. *Journal of Computational Physics*, 192:593–623, 2003.
- [24] R Mittal, H Dong, M Bozkurtas, and F M Najjar. A versatile sharp interface immersed boundary method for incompressible flows with complex boundaries. *Journal of Computational Physics*, 227:4825–4852, 2008.
- [25] Jungwoo Kim, Dongjoo Kim, and Haecheon Choi. An Immersed-Boundary Finite-Volume Method for Simulations of Flow in Complex Geometries. *Journal of Computational Physics*, 171:132–150, 2001.
- [26] P H Chiu, R K Lin, and Tony W H Sheu. A differentially interpolated direct forcing immersed boundary method for predicting incompressible Navier Stokes equations in time-varying complex geometries. *Journal of Computational Physics*, 229(12):4476–4500, 2010.
- [27] P H Chiu, Tony W H Sheu, and R K Lin. An effective explicit pressure gradient scheme implemented in the two-level non-staggered grids for incompressible Navier Stokes equations. *Journal of Computational Physics*, 227:4018–4037, 2008.